TWO SCENARIOS FOR THE FORMATION OF CUSPY DENSITY PROFILES IN ELLIPTICAL GALAXIES

F. Cruz and H. Velázquez

Instituto de Astronomía
Universidad Nacional Autónoma de México, Ensenada, B. C., México

RESUMEN

Hemos abordado la formación de perfiles agudos a través de simulaciones de N-cuerpos, en dos escenarios complementarios: (1) un colapso gravitacional frío alrededor de un agujero negro supermasivo preexistente, y (2) un crecimiento adiabático de un agujero negro en un sistema estelar relajado obtenido de un colapso gravitacional frío. Ambos modelos dan lugar a un perfil de densidad, ρ^γ, con un índice de ley de potencias similar, γ; sin embargo, presentan diferencias cinemáticas y morfológicas.

ABSTRACT

We address the formation of cuspy density profiles, through N-body simulations, in two complementary scenarios: (1) a cold gravitational collapse around a preexisting supermassive black hole, and (2) an adiabatic growth of a central black hole in a relaxed stellar system obtained from a cold gravitational collapse. Both models lead to a density profile, ρ^γ, with a similar power-law index, γ; however, they show kinematical and morphological differences.

Key Words: **GALAXIES: ELLIPTICAL AND LENTICULAR, CD — GALAXIES: FORMATION — GALAXIES: NUCLEI — METHODS: NUMERICAL**

1. INTRODUCTION

It is currently believed that the central region of galaxies harbors a supermassive black hole as, for instance, it is observed in the nuclear activity of the AGN's (Kormendy & Richstone 1995). The *Hubble Space Telescope* has substantially increased the quality and resolution of the observations of the central region of galaxies allowing a better determination of the central density profile. These data have showed that bright ellipticals have a flatter inner profile, ρ^γ, with a power-law index in the range of $0 \lesssim \gamma \lesssim 1.5$, while fainter ellipticals tend to be more cuspy with a power-law index between $1.5 \lesssim \gamma \lesssim 2$ (Crane et al. 1993; Ferrarese et al. 1994; Gebhardt et al. 1996).

In the most accepted scenario for explaining these observations, the galaxy forms first and after that a central black hole grows adiabatically producing a cuspy density profile (Peebles 1972; Young 1980; van der Marel 1999; Merritt & Quinlan 1998; Holley-Bockelmann et al. 2002). On the other hand, Stiavelli (1998) adopted the opposite scenario, a preex-

isting black hole acts a seed around which the galaxy forms through violent relaxation. He found results similar to those of the adiabatic growth model thus making it difficult to discern between them. In a recent paper, Cruz & Velázquez (2004) addressed the formation of cuspy density profiles using N-body simulations and adopting the model proposed by Stiavelli (1998). They found that a preexisting supermassive black hole is able to produce a steep inner cusp depending on the initial mass of the central black hole.

The aim of this paper is to compare both scenarios through N-body simulations. For this purpose, the central density profile, the kinematics and the morphology are compared. The rest of the paper has been organized as follows: in §2 a description of the method and the initial conditions are provided. The results are given in §3 and, finally, in §4 a discussion of the results is provided.

2. NUMERICAL METHODS

In this section, we briefly summarize the methods and initial conditions used for our numerical simulations.

2.1. *Scenario A: Primordial Black Hole*

For the cold gravitational collapse, we adopt the scheme of Aguilar & Merritt (1990) where the initial positions of the particles are obtained from the following power-law density profile:

$$\rho(r) = \frac{M_g}{2\pi R_0^3}\left(\frac{R_0}{r}\right). \tag{1}$$

Here, M_g and R_0 are the initial mass and radius of the sphere, respectively. The velocities are randomly drawn from the following distribution function:

$$f = \frac{\rho(r)}{\sqrt{2}\pi^{3/2}\sigma_r\sigma_\perp^2}\exp\left(-\frac{u^2}{2\sigma_r^2}\right)\exp\left(-\frac{j^2/r^2}{\sigma_\perp^2}\right), \tag{2}$$

where σ_r and $\sigma_\perp$ are dispersion velocities in the radial and tangential directions, respectively. j and u are the specific angular momentum and the radial velocity. An anisotropy parameter is defined as $\beta \equiv 2T_r/T_\perp$ or, equivalently, as $2\sigma_r/\sigma_\perp$, where T_r and $T_\perp$ are the kinetic energies in radial and tangential motions, respectively. The gravitational collapse begins from quite cold initial conditions with a virial ratio of $\eta \equiv 2T/|W| = 0.05$ and an anisotropy parameter of $\beta = 1$. Simulations with $32,000$ and $64,000$ equal-mass particles are used.

For these numerical experiments we have chosen a system of units such that $G = 1$, $M = 1$ and a total energy of $E = -1/4$. With this system of units, the free-fall timescale is about $t_{ff} \approx 5$ time units. Finally, for the central supermassive black hole we have adopted a point particle with a mass of $M_{bh} = 0.01$ and the simulations were allowed to evolve for about $5\,t_{ff}$.

2.2. *Scenario B: Adiabatic Growth of a Black Hole*

In this case, the cold gravitational collapses of the previous section were allowed to relax for about $5\,t_{ff}$ without a supermassive black hole (see models $GC00$ and $GC01$ in Table 1). Figure 1 shows the evolution of the Lagrangian radii for model $GC01$ for 0.1%, 1%, 5%, 10% and 50% of the mass. It is clearly seen that they remain almost constant. This also can be appreciated in the shape of the relaxed system in Figure 2 where the axis ratios b/a and c/a for 10% and 50% (half-mass radius) of the mass have been plotted. Notice that, for the last $2\,t_{ff}$, the system remains almost unchanged inside the half-mass
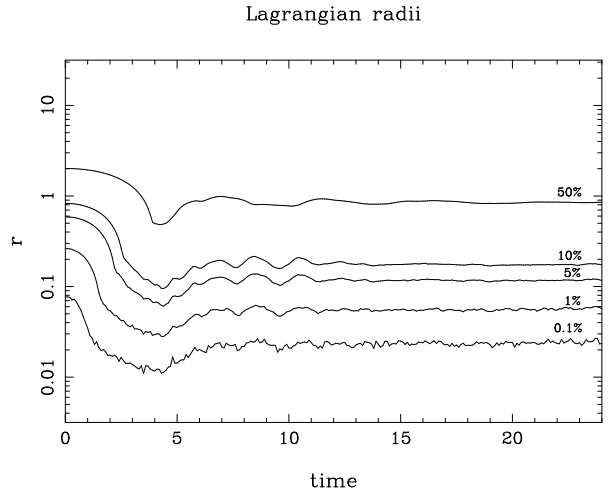

Fig. 1. Time evolution of the Lagrangian radii for the initial model $CG01$ for 0.1%, 1%, 5%, 10%, and 50% of the total mass. Notice that they remain almost constant, suggesting that the system is in steady state.

radius and for the inner region just a slight evolutionary trend is observed. From these results, we assume that the model is in near equilibrium. This condition of equilibrium is taken as our start point, $t = 0$, for the adiabatic growth of a central black hole in our numerical models $AG01$ and $AG02$ for 32,000 and 64,000 particles, respectively. At this time they exhibit an almost flat inner core with a power-law index of about 0.2. A central particle grows according to the following rule given by Merritt & Quinlan (1998):

$$\begin{aligned} M(t) &= M_{bh}\tau^2(3-2\tau), \tau \le 1, \\ &= M_{bh}, \qquad\qquad \tau > 1, \end{aligned} \tag{3}$$

where $\tau = t/t_{grow}$. For this paper we use $M_{bh} = 0.01$ and $t_{grow}=15$. Once t_{grow} is reached, we let the system relax for another $7\,t_{ff}$ (see models $AG01$ and $AG02$ in Table 1).

The rest of the parameters characterizing our N-body simulations are indicated in Table 1. Here, r_h represents the half-mass radius of the final relaxed system (just bound particles are taken into account), γ indicates the final logarithmic power-law slope of the central cusp, $r_{bh} \equiv GM_{bh}/\sigma^2$ corresponds to the black hole's radius of influence and r_{bh}^* is the radius containing in stars twice the black hole mass.

2.3. *The N-Body Code*

For the evolution and formation of steep inner cusps in both scenarios we use a direct-summation Systolic code. It has the advantage of combining

TABLE 1

INITIAL PARAMETERS AND SOME FINAL DATA

Simulation	Initial Parameters			Final Data					
	M_{bh}/M_{gal} $(\times 10^{-2})$	t_{growth}	N $(\times 10^3)$	r_{bh} $(\times 10^{-2})$	r_{bh}^* $(\times 10^{-2})$	r_h	σ_h	M_{bh}/M_{gal} $(\times 10^{-2})$	γ
GC00	0.0	...	32	...	...	0.58	0.94	...	0.1
GC01	0.0	...	64	...	...	0.54	0.97	...	0.1
GC02	1.0	...	32	1.	8.5	0.57	0.99	1.13	1.5
GC03	1.0	...	64	1.	8.6	0.59	0.97	1.14	1.5
AG01	1.12	15	32	1.	8.0	0.59	0.98	1.03	1.5
AG02	1.12	15	64	1.	8.0	0.53	1.0	1.02	1.5

a fourth-order Hermite integrator, individual time-steps and an accuracy parameter to determine the individual time-steps (Dorband, Hemsendorf, & Merritt 2003). These properties allow us to encompass a large dynamical range (both spatial and temporal) with enough accuracy. This is even more important
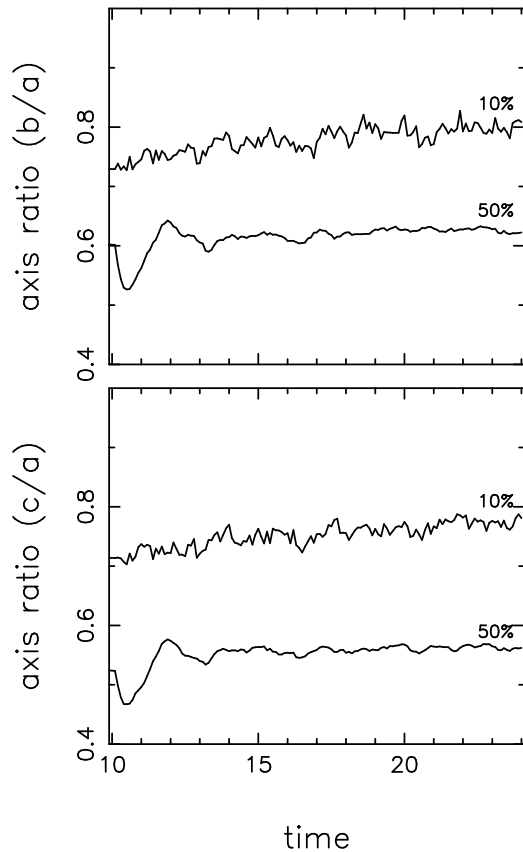

Fig. 3. Final logarithmic density profiles for models *GC*03 (thin line) and *AG*02 (thick line). The arrows correspond to r_{bh} and r_{bh}^* (see text).

Fig. 2. Time evolution of the axis ratios of the model *CG*01 in the absence of a black hole after cold collapse.These axis ratios were computed for 10% and 50% of the mass of the system.
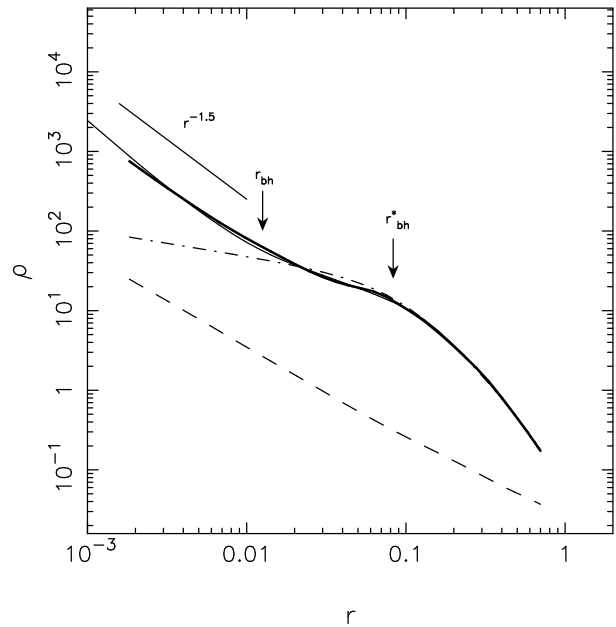
in the inner regions where the orbits of the particles inside the black hole's radius of influence need to be integrated with high accuracy. Also, the code has been optimized for parallel computers and uses MPI. In all cases energy conservation was better than 0.001%.

These numerical simulations were run on a cluster consisting of 32 processor Pentium III of 450 MHz (Velázquez & Aguilar 2003). A single simulation with 64,000 particles in this cluster takes about 2 months of CPU time.
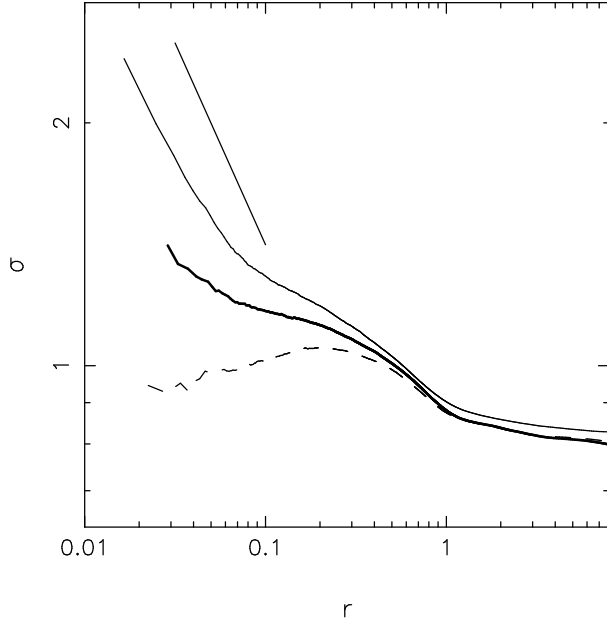
Fig. 4. Final velocity dispersion for models GC03 (thin line) and AG02 (thick line). The dashed line is the velocity dispersion for the model GC01, before the black hole starts to grow. The reference line has a logarithmic slope of $-1/2$.

3. RESULTS

The final density profiles for our N-body simulations GC03 and AG02 are plotted in Figure 3. These density profiles were computed using MAPEL (Merritt & Tremblay 1994). The thick line corresponds to the cold gravitational collapse with a primordial supermassive black hole, the thin line to the adiabatic growth of the central black hole. The long-dashed line indicates the initial density profile for the cold gravitational collapse around the supermassive black hole and the dot-dashed line corresponds to the adiabatic growth scenario. The arrow roughly shows the black hole's radius of influence. We can notice that the final density profiles are quite similar in both cases and they end up having a logarithmic slope of $\gamma \approx 1.5$. These results are in agreement with those found by Stiavelli (1998).

The final logarithmic slope, γ, the velocity dispersion, σ_h, at the half-mass radius, r_h, the radius of influence, r_{bh}, and r_{bh}^*, have been computed for all our simulations and are listed in Table 1. It can be seen that similar results are obtained for the numerical simulations with $32,000$ and $64,000$ particles.

Some differences in the kinematics of the inner regions can be appreciated in Figure 4. Here, the thin solid line corresponds to the dispersion velocity for the adiabatic growth model and the primordial
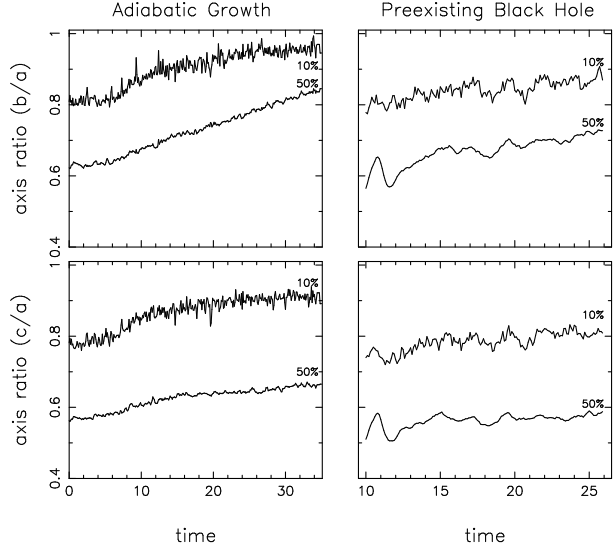

Fig. 5. Evolution of the axis ratios b/a (top panels) and c/a (bottom panels), for AG02 and GC03 simulations with 64,000 particles, for the mass percentage indicated on the right of each line.

black hole model is indicated by a thick solid line. The long-dashed line shows the initial velocity dispersion for the adiabatic model. The initial velocity dispersion for the primordial model is about an order of magnitude lower. As a reference a straight line with a logarithmic slope of $-\frac{1}{2}$ has been included. Clearly, the adiabatic growth model, in comparison with the primordial model, exhibits a velocity dispersion profile with a steeper cusp, $\sigma \sim r^{-1/2}$, as expected for particles moving under the influence of an inverse-square law. Furthermore, the velocity dispersion in the adiabatic model is about 40% larger.

Figure 5 shows the time evolution of the shape for our numerical simulations AG02 and GC03. To have a global view, the axis ratios, b/a and c/a, have been computed for the inner region, comprising 10% of the particles, and at the half-mass radius. The results for all our numerical simulations after 25 time units are summarized in Table 2. The triaxiality parameter, T, was defined as in Franx, Illingworth, & de Zeeuw (1991):

$$ T = \frac{a^2 - b^2}{a^2 - c^2} \,, \qquad (4) $$

where the limiting cases $T = 0$ and $T = 1$ correspond to oblate and prolate shapes, respectively. It can be observed that the final configurations tend to be prolate triaxial shapes at the external parts while the inner parts show more spheroidal shapes.

TABLE 2

SHAPE PARAMETERS AFTER ABOUT 25
TIME UNITS

Simulation	b/a	c/a	T
	10%, 50%	10%, 50%	10%, 50%
GC00	0.79, 0.60	0.76, 0.53	0.88, 0.89
GC01	0.80, 0.62	0.78, 0.56	0.91, 0.89
GC02	0.86, 0.72	0.83, 0.59	0.83, 0.73
GC03	0.89, 0.72	0.82, 0.59	0.63, 0.73
AG01	0.95, 0.80	0.90, 0.66	0.51, 0.63
AG02	0.94, 0.84	0.89, 0.66	0.55, 0.52

4. DISCUSSION AND CONCLUSIONS

We have found that both scenarios are capable of producing cuspy density profiles in the central regions of our models. Even more, the logarithmic slope inside the black hole's radius of influence is indistinguishable in both cases (see Table 1). These results are in general agreement with those of Stiavelli (1998) and Merritt & Quinlan 1998. Hence, the power-law index alone does not allow us to discriminate between both scenarios.

However, as we examine their kinematics and shapes some differences begin to emerge. In both scenarios the velocity dispersion σ is comparable in the regions outside the half-mass radius, but in the inner regions around the black hole's radius of influence some important differences can be appreciated. The adiabatic growth scenario forms a more cuspy velocity profile with a radial dependence given by $\sigma \sim r^{-1/2}$ and with a central value 40% larger than in the primordial case.

Furthermore, the effect of the central mass extends beyond the radius of influence of the black hole. From Table 2 we can see that: (1) cold gravitational collapses in the absence of a central massive particle show more prolate shapes and (2), the adiabatic growth of a central black hole exhibits more slightly spheroidal systems than the primordial case.

Nevertheless, we see a general tendency towards an axisymmetric shape with $b/a \to 1$ at later times (see Fig. 5). This evolution is likely due to the mechanism mentioned by Merritt & Quinlan (1998): stochasticity is induced by the central supermassive black hole, resulting from the loss of two of the three integrals of motion of regular box orbits that support a triaxial shape. By the end, these box orbits are replaced by tube-like orbits.

To have a better understanding of their kinematics and morphology is necessary to study, in detail, the orbital structure of these systems. However, this is out of the scope of the present work; we are working in this direction and the results will appear in a forthcoming paper.

REFERENCES

Aguilar, L., & Merritt, D. 1990, ApJ, 354, 33
Crane, P., et al. 1993, AJ, 106, 1371
Cruz, F., & Velázquez, H. 2004, ApJ, 612, 593
Dorband, N., Hemsendorf, M., & Merritt, D. 2003, J. Comp. Phys., 185, 484
Ferrarese, L, van den Bosch, F. C., Ford, H. C., Jaffe, W., & O'Connell, R. W. 1994, AJ, 108, 1598
Franx, M., Illingworth, G., & Zeeuw, T. 1991, ApJ, 383, 112
Gebhardt, K., et al. 1996, AJ, 112, 105
Holley-Bockelmann, K., Mihos, J. C., Sigurdsson, S., Hernquist, L., & Norman, C. 2002, ApJ, 567, 817
Kormendy, J., & Richstone, D. 1995, ARA&A, 33, 581
Merritt, D., & Quinlan, Q. 1998, ApJ, 498, 625
Merritt, D., & Tremblay, B. 1994, AJ, 108, 514
Peebles, P. J. E. 1972, General Relativ. Gravitation, 3, 63
Stiavelli, M. 1998, ApJ, 495, L91
Velázquez, H,. & Aguilar, L. 2003, RevMexAA, 39, 197
van der Marel, R. P. 1999, AJ, 117, 744
Young, P. 1980, ApJ, 242, 1232

Fidel Cruz and Héctor Velázquez: Instituto de Astronomía, UNAM, Apdo. Postal 877, 22800 Ensenada, B. C., México   (fidel@astrosen.unam.mx; hmv@astrosen.unam.mx).